Reactive Power Compensation and Negative-Sequence Current Suppression System for Electrical Railways With YNvd-Connected Balance Transformer—Part II: Implementation and Verification

Bin Xie, Zhiwen Zhang, Yong Li, *Senior Member, IEEE*, Sijia Hu, *Member, IEEE*, Longfu Luo, *Member, IEEE*, Christian Rehtanz, *Senior Member, IEEE*, and Olav Krause, *Member, IEEE*

***Abstract*—This part mainly focuses on the implementation and verification of the reactive power compensation and negative-sequence current suppression system with YNvd-connected balance transformer, by means of simulation and experiment. The system model is presented, and a current control method, which explores the dissipation characteristic of the proposed system under two-phase rotating frame, is analyzed. Then, a stability analysis of this control is made, considering the deviations of system parameters and the time delay caused by the low-pass filter. Besides, dc-link overall control and balance control are investigated, and the self-balance ability of multiple dc links is briefly discussed. Both the simulation and experimental results verify the effectiveness of the proposed system topology, compensation strategy, and control method.**

***Index Terms*—Balance transformer, converter, dissipation-characteristic-based control, electrical railway power system (ERPS), power quality.**

I. Introduction

FOR cost-efficiency consideration, the single-phase supply systems with industrial frequency 50 Hz (or 60 Hz) are widely adopted in the electrical railway power systems (ERPS) worldwide [1]. However, the locomotives cause considerable negative-sequence current (NSC) on the three-phase high-voltage grid due to its unbalanced distribution on feeders, which brings negative influence on the sensitive power consumers and generators [2], [3]. Besides, the conventional phase-controlled trains draw a significant amount of reactive power from and also inject plenty of low-order harmonic currents into the utility, which leads to undesired energy consumptions and setup damages [4]. On the other hand, as the wide applications of the pulse width modulation technique-based new generation trains, less reactive power and low-order harmonics are obtained in some ERPS sections [5], but the unbalance issue may be deteriorated for its higher power level than the conventional one, so do the high-order harmonics resonances [6], [7]. Much attention has been paid to the above ERPS power quality problems these years [8].

For some projects with restricted investment, the passive methods, e.g., the *LC*-branches, which are adopted to deal with the harmonic or reactive power related problems, are attractive to engineers [9]. Considering the fixed compensating characteristic and resonance risk, the value of the L and C components should be designed carefully [10], [11].

Compared to the above discussed passive methods, active solutions are superior in working performance and installation area [12], [13]. Active power filters (APF) have a good harmonic suppressing ability but a relatively high switching frequency is required to obtain a satisfactory working bandwidth [14], which becomes an obstacle for its application in medium-voltage (MV) systems in some extent. Benefits from the multilevel technology, static synchronous compensators (STATCOM) [15], [16], and unified power quality conditioners (UPQC) [17]–[19] are widely used in MV systems to deal with the power quality or stability-related problems. Many control methods [20], which mainly involve the instantaneous power theory and synchronous rotating reference frame, can integrate with those active systems. However, for ERPS, those apparatus always cannot be directly applied [21]. A system called active power quality compensator (APQC), with a three-phase converter integrating into the two-phase feeders via a Scott transformer, was proposed in [22].

Manuscript received August 19, 2016; revised October 30, 2016 and December 4, 2016; accepted January 9, 2017. Date of publication February 1, 2017; date of current version August 2, 2017. This work was supported in part by the National Nature Science Foundation of China under Grant 51477046 and Grant 51377001, and in part by the International Science and Technology Cooperation Program of China under Grant 2015DFR70850. Recommended for publication by Associate Editor Z. Li. *(Corresponding authors: Z. Zhang and Y. Li.)*

B. Xie, Z. Zhang, Y. Li, S. Hu, and L. Luo are with the College of Electrical and Information Engineering, Hunan University, Changsha 410082, China (e-mail: xiebin_1215@163.com; hdzzw@126.com; yongli@hnu.edu.cn; huda_hsj@163.com; llf@hnu.edu.cn).

C. Rehtanz is with the Institute of Energy Systems, Energy Efficiency and Energy Economics, TU Dortmund University, Dortmund 44227, Germany (e-mail: christian.rehtanz@tu-dortmund.de).

O. Krause is with the School of Information Technology and Electrical Engineering, The University of Queensland, Brisbane, Qld. 4072, Australia (e-mail: o.krause@uq.edu.au).

Color versions of one or more of the figures in this paper are available online at http://ieeexplore.ieee.org.

Digital Object Identifier 10.1109/TPEL.2017.2662379

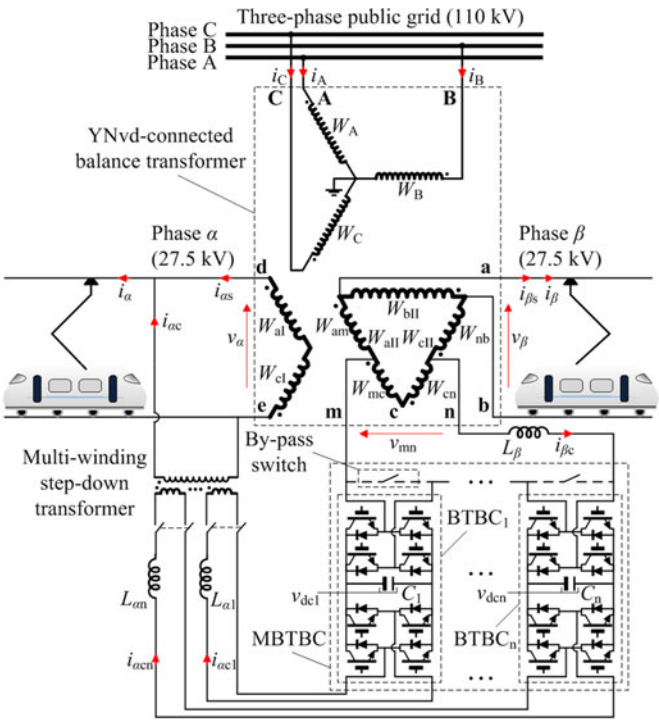

Fig. 1. Topology of the proposed system.

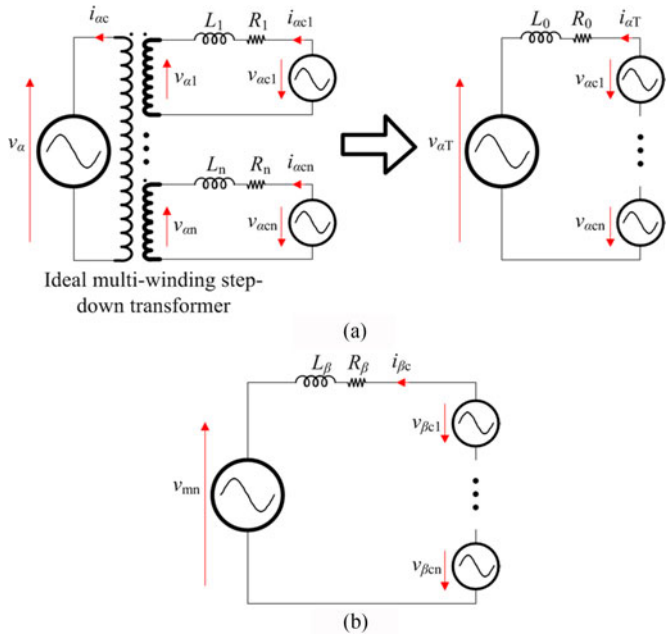

Fig. 2. Equivalent circuits of the (a) phase-α converter and (b) phase-β converter.

The added auxiliary Scott transformer greatly increases the cost and installing space of the whole system. Besides, the adopted hysteretic control method also has some inherent disadvantages in MV-level applications [14]. A three-phase voltage-source converter utilizing direct power control scheme for harmonic and unbalance compensation in ERPS was proposed in [23]. Similar to APQC, this converter requires a high-power insolation transformer as an interface of the primary high-voltage grid. In [24] and [25], by employing the specifically designed taps on the multipurpose balance transformer, a three-phase converter can be directly integrated (or via some specifically designed *LC*-branches) into the main transformer's secondary windings for a satisfactory power quality improvement in ERPS. While selecting the optimal gains $\boldsymbol{K}_{\rm opt}$ of the proposed linear quadratic regulator with integral action may become a challenge for the controller designing engineers [24]. Evolved from UPQC or STATCOM, two back-to-back-connected single-phase converters, i.e., the well-known railway static power conditioner (RPC) [26], [27], can be applied for power balance, reactive compensation, and harmonic elimination in ERPS, and some control methods aiming to reduce RPC's designing capacity was also proposed in [28] to further improve its cost efficiency. However, two single-phase multiwinding step-down transformers are indispensable.

In this paper, a novel system constructed with multiplex back-to-back converters (MBTBC) is proposed. It can be seen from Fig. 1 that the loads (i.e., trains) on phase α and β are fed by the terminals d-e and a-b of the YNvd-connected balance transformer. By taking the advantage of the natural asymmetry between the "v" and "Δ" windings, MBTBC can connect with d-e via a single-phase multiwinding step-down transformer with the parallel constructed units in the one side; on the other side, a multilevel topology is adopted for the connection of taps m and n. So, different from conventional RPC scheme, only one insolation transformer is required in the proposed system. The improvement on topology together with the ingenious designed partial compensation strategy presented in the first part of this topic makes the system compact, modular, and flexible though the design of the main transformer of the proposed system is a little more difficult than the Vv traction transformer [2] (but easier than the commonly used impedance-matching transformer [24]). Since the detailed topology introduction, compensation principle, and new partial compensation strategy are presented in the first part of this paper, so the implementation and verification of the proposed system are the main tasks of this part. For implementation, the dissipation characteristic of a general circuit-based control method [29], which has been reported in STATCOM [30], hybrid APF [31], and ERPS [32], [33], is applied to control MBTBC. Different from those three-phase applications of the method, it is analyzed for single-phase application and the related stability problems are also discussed in detail in this paper. This paper is organized as follows. In Section II, the system model is briefly introduced. The current control scheme, related stability problems, and dc-link voltage control mechanism are discussed in Section III. In Section IV, the simulation and experimental results are fully demonstrated. Finally, a conclusion is drawn in Section V.

II. System Modeling

Fig. 2 shows the related equivalent circuits (the linkage impedances of transformer are considered in link branches) of the proposed system shown in Fig. 1 (note: in Fig. 2, $v_{\alpha 1}$ +

$v_{\alpha 2} + \ldots v_{\alpha \mathrm{n}} = x v_\alpha$, $v_{\mathrm{mn}} = x v_\beta$, and $x = W_{\mathrm{mc}}/W_{\mathrm{a\,II}}$). For discussing convenience, only the fundamental component of converter's output voltage is used in the following discussion.

The equivalent circuit of the n-level parallel-connected converter of MBTBC can be degenerated from the left one in Fig. 2(a) to the right one, which is the same with the circuit of the phase-β converter shown in Fig. 2(b), if it holds: $L_0 = \mathrm{n}L_1 = \ldots = \mathrm{n}L_{\mathrm{n}}$, $R_0 = \mathrm{n}R_1 = \ldots = \mathrm{n}R_{\mathrm{n}}$, $v_{\alpha \mathrm{T}} = x v_\alpha$, and $i_{\alpha \mathrm{T}} = i_{\alpha \mathrm{c}}/x$.

Let $L_0 = L_\beta = L$ and $R_0 = R_\beta = R$, one can obtain

$$v_{\alpha T} + L di_{\alpha T}/dt + R i_{\alpha T} = v_{\alpha c} \tag{1}$$

$$v_{mn} + L di_{\beta c}/dt + R i_{\beta c} = v_{\beta c} \tag{2}$$

where $v_{\alpha \mathrm{c}} = v_{\alpha \mathrm{c}1} + v_{\alpha \mathrm{c}2} + \ldots v_{\alpha \mathrm{cn}}$ and $v_{\beta \mathrm{c}} = v_{\beta \mathrm{c}1} + v_{\beta \mathrm{c}2} + \ldots v_{\beta \mathrm{cn}}$.

Though, $i_{\alpha \mathrm{T}}$ and $i_{\beta \mathrm{c}}$ are interacted each other due to the active power exchange of both sides' converters, the control implementation of $i_{\alpha \mathrm{T}}$ and $i_{\beta \mathrm{c}}$ can be carried out independently considering the energy-buffering effect of the dc-link capacitors.

III. Control Algorithm

A. Current Control

Considering that the active and reactive components of the reference currents can be calculated by the new partial compensation strategy proposed in the first part of this paper, here, the currents and voltages in (1) are expressed as

$$\begin{cases} v_{\alpha T} = V_{\alpha T} \cos(\omega t) = V_{\alpha T p} \cos(\omega t) \\ i_{\alpha T} = I_{\alpha T p} \cos(\omega t) + I_{\alpha T q} \sin(\omega t) \\ v_{\alpha c} = V_{\alpha c p} \cos(\omega t) + V_{\alpha c q} \sin(\omega t) \end{cases} \tag{3}$$

where $I_{\alpha \mathrm{Tp}}$, $V_{\alpha \mathrm{cp}}$ and $I_{\alpha \mathrm{Tq}}$, $V_{\alpha \mathrm{cq}}$ are the amplitudes of the active and reactive components of the corresponding current and voltage, respectively; $\cos(\omega t)$ and $\sin(\omega t)$, which rely on phase-locked loop (PLL) is used in Fig. 6, represent the active and reactive directions of the phase-α converter.

Inserting (3) into (1), the parts on active and reactive directions satisfy

$$\begin{cases} L dI_{\alpha T p}/dt + L\omega I_{\alpha T q} + R I_{\alpha T p} = V_{\alpha c p} - V_{\alpha T p} \\ L dI_{\alpha T q}/dt - L\omega I_{\alpha T p} + R I_{\alpha T q} = V_{\alpha c q} \end{cases}. \tag{4}$$

For discussion convenience, (4) is rewritten as

$$\mathbf{D}p\mathbf{x} + \mathbf{J}\mathbf{x} + \mathbf{R}\mathbf{x} = \mathrm{v}_{\alpha c} - \mathrm{v}_{\alpha T} \tag{5}$$

where $\mathrm{D} = \left[\begin{smallmatrix} L & 0 \\ 0 & L \end{smallmatrix}\right]$, $\mathrm{J} = \left[\begin{smallmatrix} 0 & \omega L \\ -\omega L & 0 \end{smallmatrix}\right]$, $\mathrm{R} = \left[\begin{smallmatrix} R & 0 \\ 0 & R \end{smallmatrix}\right]$, $\mathrm{x} = \left[\begin{smallmatrix} I_{\alpha T p} \\ I_{\alpha T q} \end{smallmatrix}\right]$, $\mathrm{v}_{\alpha c} = \left[\begin{smallmatrix} V_{\alpha c p} \\ V_{\alpha c q} \end{smallmatrix}\right]$, $\mathrm{v}_{\alpha T} = \left[\begin{smallmatrix} V_{\alpha T p} \\ 0 \end{smallmatrix}\right]$, and p is the differential operator.

On the other hand, if the control variables track their references without steady-state error, (5) can also be written as

$$\mathbf{D}p\mathbf{x}^* + \mathbf{J}\mathbf{x}^* + \mathbf{R}\mathbf{x}^* = \mathrm{v}_{\alpha c}{}^* - \mathrm{v}_{\alpha T} \tag{6}$$

where $\mathrm{x}^* = \left[\begin{smallmatrix} I_{\alpha T p}{}^* \\ I_{\alpha T q}{}^* \end{smallmatrix}\right]$ and $\mathrm{v}_{\alpha c}{}^* = \left[\begin{smallmatrix} V_{\alpha c p}{}^* \\ V_{\alpha c q}{}^* \end{smallmatrix}\right]$ are corresponding references.

In order to evaluate the currents' tracking performance, an energy function E (note: $E \geq 0$) is defined as

$$\begin{aligned} E &= 0.5L((I_{\alpha T p} - I_{\alpha T p}{}^*)^2 + (I_{\alpha T q} - I_{\alpha T q}{}^*)^2) \\ &= 0.5\tilde{\mathbf{x}}^T \mathbf{D}\tilde{\mathbf{x}} \end{aligned} \tag{7}$$

where $\tilde{\mathrm{x}} = \mathrm{x} - \mathrm{x}^* = \left[\begin{smallmatrix} I_{\alpha T p} - I_{\alpha T p}{}^* \\ I_{\alpha T q} - I_{\alpha T q}{}^* \end{smallmatrix}\right]$.

It can be observed from (7) that good tracking performance of $\mathbf{x}$ will lead to small E. That is to say, the tracking speed can be evaluated by the change rate of E, i.e., pE. According to the Lyapunov theorem, if

$$pE \leq -\tau E < 0,\ \tau > 0 \tag{8}$$

E will exponentially converge to zero, which means a good current tracking performance is obtained. Besides, the convergence speed is determined by τ.

Considering (7), pE can be derived as

$$pE = \tilde{\mathbf{x}}^T \mathbf{D} p \tilde{\mathbf{x}}. \tag{9}$$

Subtracting (6) from (5), one can obtain that

$$\mathbf{D}p\tilde{\mathbf{x}} + \mathbf{J}\tilde{\mathbf{x}} + \mathbf{R}\tilde{\mathbf{x}} = \tilde{\mathrm{v}}_{\alpha c} \tag{10}$$

where $\tilde{\mathrm{v}}_{\alpha c} = \mathrm{v}_{\alpha c} - \mathrm{v}_{\alpha c}{}^* = \left[\begin{smallmatrix} V_{\alpha c p} - V_{\alpha c p}{}^* \\ V_{\alpha c q} - V_{\alpha c q}{}^* \end{smallmatrix}\right]$.

Inserting (10) into (9), pE can be calculated as

$$pE = -\tilde{\mathbf{x}}^T \mathbf{R}\tilde{\mathbf{x}} + \tilde{\mathbf{x}}^T \tilde{\mathbf{v}}_{\alpha c}. \tag{11}$$

If $\tilde{\mathrm{v}}_{\alpha c}$ in (11) equals to $\mathbf{0}$, i.e.,

$$\mathrm{v}_{\alpha c} = \mathrm{v}_{\alpha c}{}^* = \mathbf{D}p\mathbf{x}^* + \mathbf{J}\mathbf{x}^* + \mathbf{R}\mathbf{x}^* + \mathrm{v}_{\alpha T} \tag{12}$$

(8) can be definitely satisfied, i.e.,

$$pE \leq -(2R/L)E = -\tau E < 0. \tag{13}$$

So, it can be concluded that (7) can converge to zero due to the natural dissipative characteristic of the proposed system itself. The convergence speed, however, is relatively slow due to the uncontrolled and small τ (see (13)).

Note if the currents have tracked its references in steady state, (6) is satisfied. Simultaneously, one can also have

$$\tilde{\mathrm{x}} = \mathbf{0}. \tag{14}$$

Multiplying a coefficient matrix $\mathbf{B}$ in both sides of (14) leads to

$$\mathrm{B}\tilde{\mathbf{x}} = \mathbf{0} \tag{15}$$

where $\mathrm{B} = \left[\begin{smallmatrix} B & 0 \\ 0 & B \end{smallmatrix}\right]$.

Combining (15) and (6), a new equation can be obtained as

$$\mathbf{D}p\mathbf{x}^* + \mathbf{J}\mathbf{x}^* + \mathbf{R}\mathbf{x}^* - \mathbf{B}\tilde{\mathbf{x}} = \mathrm{v}_{\alpha c}{}^* - \mathrm{v}_{\alpha T}. \tag{16}$$

Similar to the derivation of (12) and (13), one can obtain (17) and (18) as follows:

$$\mathrm{v}_{\alpha c} = \mathrm{v}_{\alpha c}{}^* = \mathbf{D}p\mathbf{x}^* + \mathbf{J}\mathbf{x}^* + \mathbf{R}\mathbf{x}^* - \mathbf{B}\tilde{\mathbf{x}} + \mathrm{v}_{\alpha T} \tag{17}$$

$$pE \leq -[(2R + B)/L]E. \tag{18}$$

Comparing (13) and (18), τ changes from $2R/L$ to $(2R + B)/L$. By tuning B, a satisfied converge speed can be obtained.

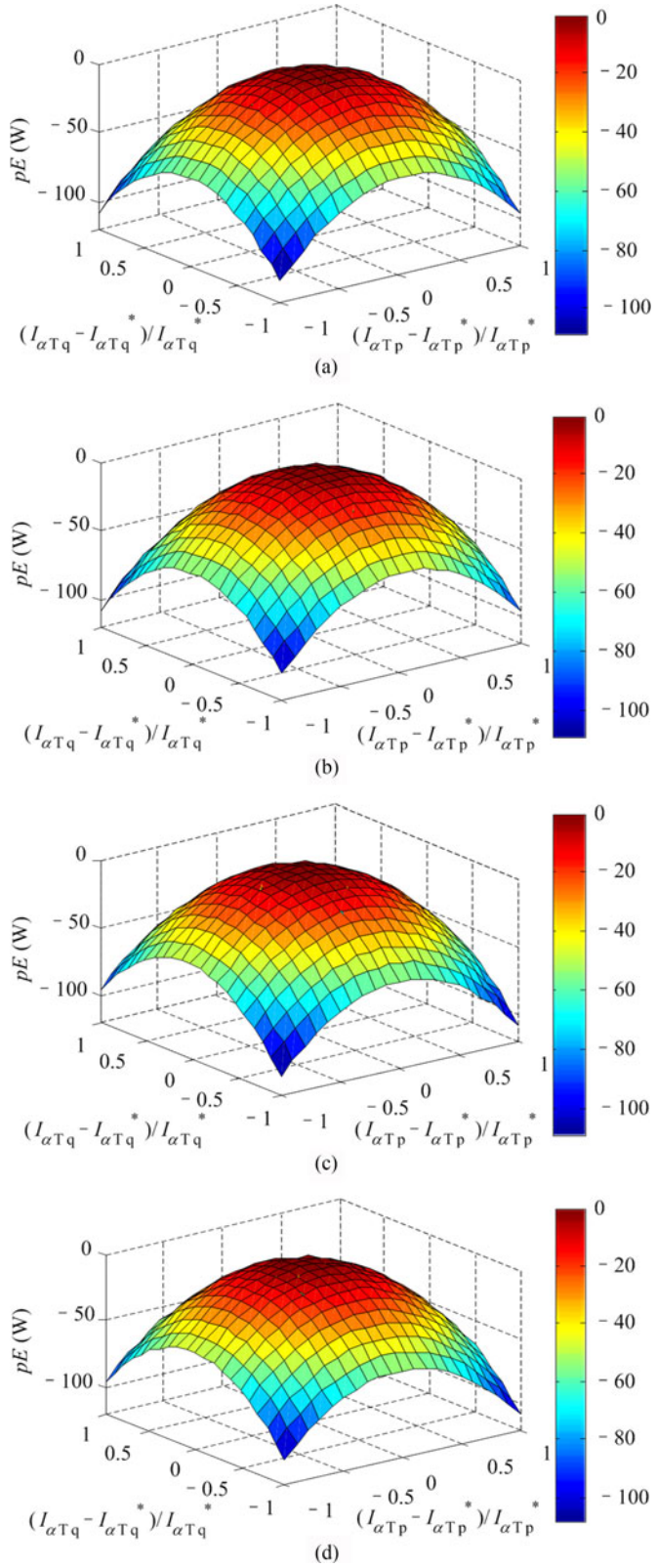

Fig. 3. Relationship between pE and the error currents on four different deviations. (a) $\Delta L = 100\%$, and $\Delta R = 100\%$. (b) $\Delta L = -100\%$, and $\Delta R = 100\%$. (c) $\Delta L = 100\%$, and $\Delta R = -100\%$. (d) $\Delta L = -100\%$, and $\Delta R = -100\%$.

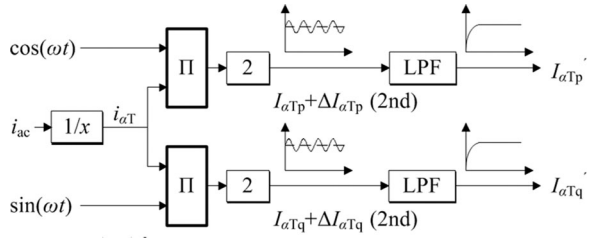

Fig. 4. Basic method for $\mathbf{x}$ acquisition.

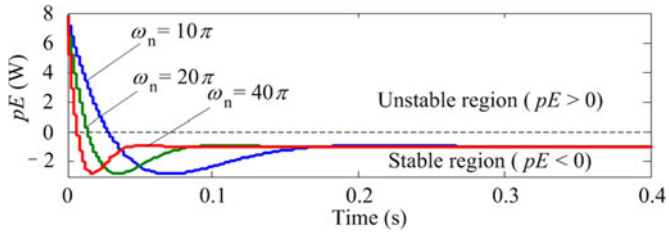

Fig. 5. Profile of pE if the delay in the acquisition of $\mathbf{x}$ is considered.

Besides, (17) also indicates that B is a virtual resistor (i.e., the unit of B is ohm (Ω)), which is connected in series with the link branch to enhance the system's dissipation performance.

Finally, $\mathbf{v}_{\alpha c}$ in (17) should be transformed into the instantaneous quantity $v_{\alpha c}$ for modulation, i.e.,

$$v_{\alpha c} = \left[\cos(\omega t)\ \sin(\omega t)\right] \mathrm{v}_{\alpha c}. \tag{19}$$

B. Stability Analysis of Current Control

Note that the derivation of the current controller is under the assumption that system's parameters have no deviations and $\mathbf{x}$ can be obtained without delay. However, the two conditions cannot be always satisfied in real applications.

1) Deviations of System Parameters: Considering the parameter disturbance, (16) can be rewritten as

$$\begin{aligned}&(\mathbf{D}+\Delta\mathbf{D})p\mathbf{x}^* + (\mathbf{J}+\Delta\mathbf{J})\mathbf{x}^* + (\mathbf{R}+\Delta\mathbf{R})\mathbf{x}^* - \mathbf{B}\tilde{\mathbf{x}}\\ &= \mathrm{v}_{\alpha c}{}^* - (\mathrm{v}_{\alpha T} + \Delta\mathrm{v}_{\alpha T})\end{aligned} \tag{20}$$

where $\Delta\mathrm{D} = \left[\begin{smallmatrix}\Delta L & 0\\ 0 & \Delta L\end{smallmatrix}\right]$, $\Delta\mathrm{J} = \left[\begin{smallmatrix}0 & \Delta L\omega\\ -\Delta L\omega & 0\end{smallmatrix}\right]$, $\Delta\mathrm{R} = \left[\begin{smallmatrix}\Delta R & 0\\ 0 & \Delta R\end{smallmatrix}\right]$, $\Delta\mathrm{v}_{\alpha T} = \left[\begin{smallmatrix}\Delta V_{\alpha\mathrm{T}p}\\ \Delta V_{\alpha\mathrm{T}q}\end{smallmatrix}\right]$, and ΔL, ΔR, $\Delta V_{\alpha\mathrm{T}p}$, $\Delta V_{\alpha\mathrm{T}q}$ are the deviations of L, R, and the active and reactive components of $V_{\alpha\mathrm{T}}$, respectively.

Subtracting (20) from (5), one can obtain

$$\begin{aligned}&\mathbf{D}p\tilde{\mathbf{x}} + \mathbf{J}\tilde{\mathbf{x}} + (\mathbf{R}+\mathbf{B})\tilde{\mathbf{x}}\\ &= \tilde{\mathrm{v}}_{\alpha c} + \Delta\mathrm{v}_{\alpha T} + \Delta\mathbf{D}p\mathbf{x}^* + \Delta\mathbf{J}\mathbf{x}^* + \Delta\mathbf{R}\mathbf{x}^*.\end{aligned} \tag{21}$$

Combining (9) and (21), and assuming $\tilde{\mathbf{v}}_{\alpha c} = \mathbf{0}$ leads to

$$\begin{aligned}pE = &-\tilde{\mathbf{x}}^T(\mathbf{R}+\mathbf{B})\tilde{\mathbf{x}}\\ &+\tilde{\mathbf{x}}^T\Delta\mathbf{v}_{\alpha T} + \tilde{\mathbf{x}}^T(\Delta\mathbf{D}p + \Delta\mathbf{J} + \Delta\mathbf{R})\mathbf{x}^*.\end{aligned} \tag{22}$$

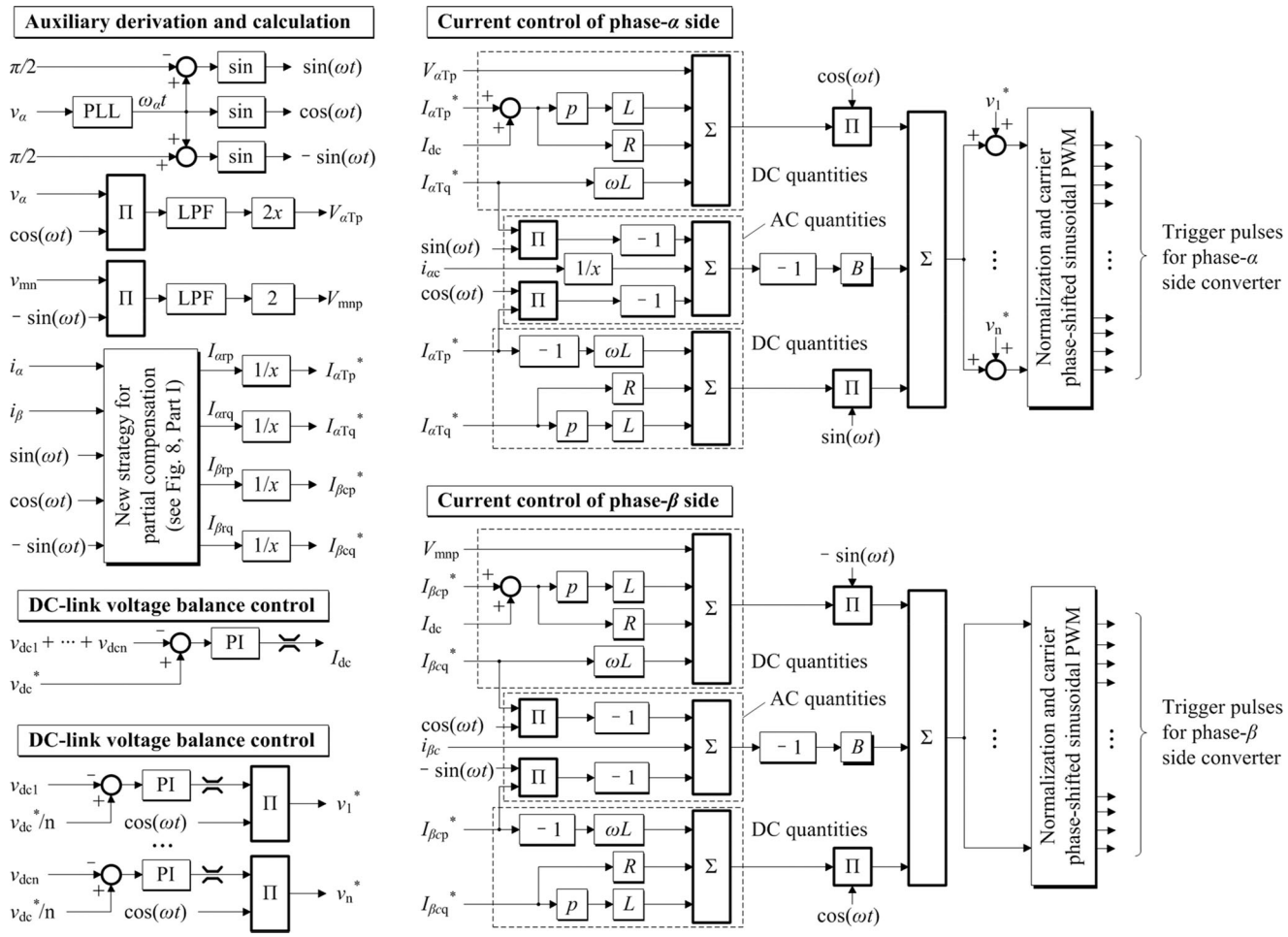

Fig. 6. Implementation of the whole control algorithm.

Considering the term $\tilde{\mathbf{x}}^T \Delta \mathbf{v}_{\alpha T}$ in (22) is much smaller than other terms, (22) can be degenerated into

$$pE = -\tilde{\mathbf{x}}^T(\mathbf{R}+\mathbf{B})\tilde{\mathbf{x}} + \tilde{\mathbf{x}}^T(\Delta \mathbf{D}p + \Delta \mathbf{J} + \Delta \mathbf{R})\mathbf{x}^*. \quad (23)$$

Let $B = 50\,\Omega$, $L = 10\,\text{mH}$, $R = 1\,\Omega$, pE is definitely negative when $\tilde{\mathbf{x}}\ /\mathbf{x}^* \in [-100\%, 100\%]$. It can be seen from Fig. 3 that the larger the $\tilde{\mathbf{x}}\ /\mathbf{x}^*$ is, the stronger the dissipation effect can be obtained, which is expected in the design of the current controller.

2) Delay in the Acquisition of $\boldsymbol{x}$*:* Fig. 4 depicts a basic $\mathbf{x}$ acquisition method, in which two low-pass filters (LPF) are involved. The transfer function of a typical second-order LPF is

$$G(s) = \frac{{\omega_n}^2}{s^2 + \frac{s\omega_n}{Q} + {\omega_n}^2} \quad (24)$$

where ω_n is the characteristic angular frequency; Q is the equivalent quality factor, $Q = 0.707$. If ω_n is set low enough, the influence of second-order ripple can be eliminated, and only the dc component is remained (see Fig. 4).

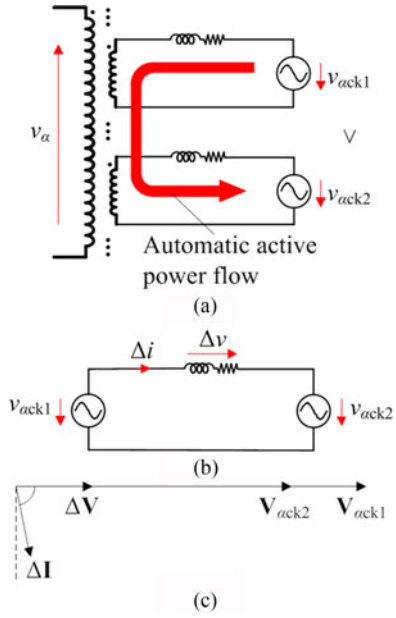

Fig. 7. Self-balance principle. (a) Self-balance topology. (b) Equivalent circuit. (c) Fundamental phasor relationships.

In frequency domain, a signal $\mathbf{x}(s)$ inputs the LPF, the output signal $\mathbf{x}'(s)$ can be obtained as

$$\mathbf{x}'(s) = \mathbf{x}(s)G(s) = \mathbf{x}\frac{{\omega_n}^2}{s(s^2 + \sqrt{2}s\omega_n + {\omega_n}^2)}. \quad (25)$$

The corresponding time-domain expression of (25) can also be expressed as

$$\mathbf{x}'(t) = \mathscr{L}^{-1}[\mathbf{x}'(s)] = \mathbf{x}\left(1 + \sqrt{2}e^{-\frac{\omega_n t}{\sqrt{2}}}\sin\left(-\frac{\omega_n t}{\sqrt{2}} - \pi/4\right)\right) \quad (26)$$

where $\mathscr{L}^{-1}$ is the reverse Laplace transformation operator.

Taking the delay of LPF into account, (16) can be rewritten as

$$\mathbf{D}p\mathbf{x}^* + \mathbf{J}\mathbf{x}^* + \mathbf{R}\mathbf{x}^* - \mathbf{B}(\mathbf{x}' - \mathbf{x}^*) = {\mathbf{v}_{\alpha c}}^* - \mathbf{v}_T. \quad (27)$$

Similar to the analysis process aforementioned, pE can be recalculated as

$$\begin{aligned} pE = & -\tilde{\mathbf{x}}^T(\mathbf{R} + \mathbf{B})\tilde{\mathbf{x}} + \tilde{\mathbf{x}}^T\mathbf{B}\mathbf{x}\sqrt{2}e^{-\frac{\omega_n t}{\sqrt{2}}} \\ & \times \sin\left(-\frac{\omega_n t}{\sqrt{2}} - \pi/4\right). \end{aligned} \quad (28)$$

Let $L = 10$ mH, $R = 1\,\Omega$, $B = 50\,\Omega$, and $\tilde{\mathbf{x}} = -10\%\mathbf{x}^*$, the profile of *pE* is shown in Fig. 5. Obviously, an unstable region is occurred ($pE > 0$). Hence, instead of the dc components in (17), the implementation of the *B* related terms should be carried out under alternating-current (ac) quantities [see the "ac quantities" block in Fig. 6].

The designing method of the converter in phase β is the same as aforementioned.

C. Overall DC-Link Voltage Control

As analyzed in the first part of this paper, the reference currents include unbalanced active power components (P_{UB}), balanced reactive power components (Q_{B}), and unbalanced reactive power components (Q_{UB}), which are responsible for delivering active power from one side of MBTBC to another side, compensating inductive reactive power for both sides, and compensating inductive reactive power for one side and compensating capacitive reactive power for another side, respectively. In order to make the whole dc-link voltage stable, a small amount of energy is delivered from the source sides to the dc link to compensate the losses of MBTBC by superposing an active power component (P_B) (i.e., I_{dc}, the output of the proportional-integral (PI) regulator for dc-link overall voltage control in Fig. 6) on P_{UB} ($I^*_{\alpha\mathrm{Tp}}$ and $I^*_{\beta\mathrm{cp}}$ in Fig. 6).

D. Unit DC-Link Voltage Balance Control

To balance the unit dc-link voltages in this paper, the energy transmission between the source side and all units dc links should be controlled. Since the parallel-connected topology on phase α allows independent units currents control ($i_{\alpha\mathrm{c}1}, \ldots, i_{\alpha\mathrm{cn}}$ in Fig. 1), so a balance control is implemented on the phase-α side (see Fig. 6).

On the other hand, though the aforementioned unit dc-link voltage balance control is adopted, it is worth to note that the proposed converter topology has unit dc-link voltage self-balance capability if the overall voltage is satisfactorily controlled. The principle is shown in Fig. 7, in which $v_{\alpha\mathrm{ck}1}$ and $v_{\alpha\mathrm{ck}2}$ are two arbitrary unit output voltages on phase-α side with the assumption $V_{\alpha\mathrm{ck}1} > V_{\alpha\mathrm{ck}2}$. Based on the equivalent circuit (see Fig. 7(b)) and phasor relationships (see Fig. 7(c)), a small amount of active power will be delivered automatically from $v_{\alpha\mathrm{ck}1}$ terminal to $v_{\alpha\mathrm{ck}2}$ terminal, as shown in Fig. 7(a), which is good for unit dc-link voltage unbalance suppression.

TABLE I
SIMULATION PARAMETERS

Items	Parameters	Value
Three-phase grid	Nominal line voltage	110 kV
	Short capacity	500 MVA
YNvd-connected balance transformer	Nominal feeder voltage	27.5 kV
	Nominal tapped winding voltage	10.5 kV
	Nominal capacity	20 MVA
Multiwinding step-down transformer	Number of secondary windings	8
	Nominal secondary voltage	1312.5 V
	Nominal Capacity	10 MVA
Inductance	$L_{\alpha 1} - L_{\alpha 8}$	1.25 mH
	L_β	10 mH
Capacitance	$C_1 - C_8$	10 mF
Controller gain	B	50 Ω
PI regulator for DC-link overall voltage control	Proportional gain	0.1
	Integral gain	3
PI regulator for DC-link voltage balance control	Proportional gain	10
	Integral gain	200
Modulator	Carrier frequency	500 Hz
DC-link voltage	Overall reference	20000 V
	Individual reference	2500 V
Load in phase α	Nominal power	5 MW + 1 MVar
Load in phase β	Nominal power	10 MW + 8 MVar

IV. SIMULATION AND EXPERIMENTAL VERIFICATION

Based on the above discussed implementation process on system modeling and controlling, the proposed system topology, compensation principle, and partial compensation strategy (see Appendix A for the defined partial compensation goals) in the first part of this paper can be verified by simulation and experiment.

A. Simulation Verification

Referring to Fig. 1, we built a simulation model by the MATLAB software. The parameters are listed in Table I.

When the simulation starts, compensation is not enabled first. The currents are unbalanced and $\mathrm{PF_f} \approx 0.8$ (see Fig. 8(a) and (b)). When the proposed partial compensation is activated at 0.1 s, $\mathrm{PF_f}$ improves to about 0.9 and I_{unb} decreases to about 0.1, respectively. Note that the $\mathrm{PF_f}$ in this paper is a

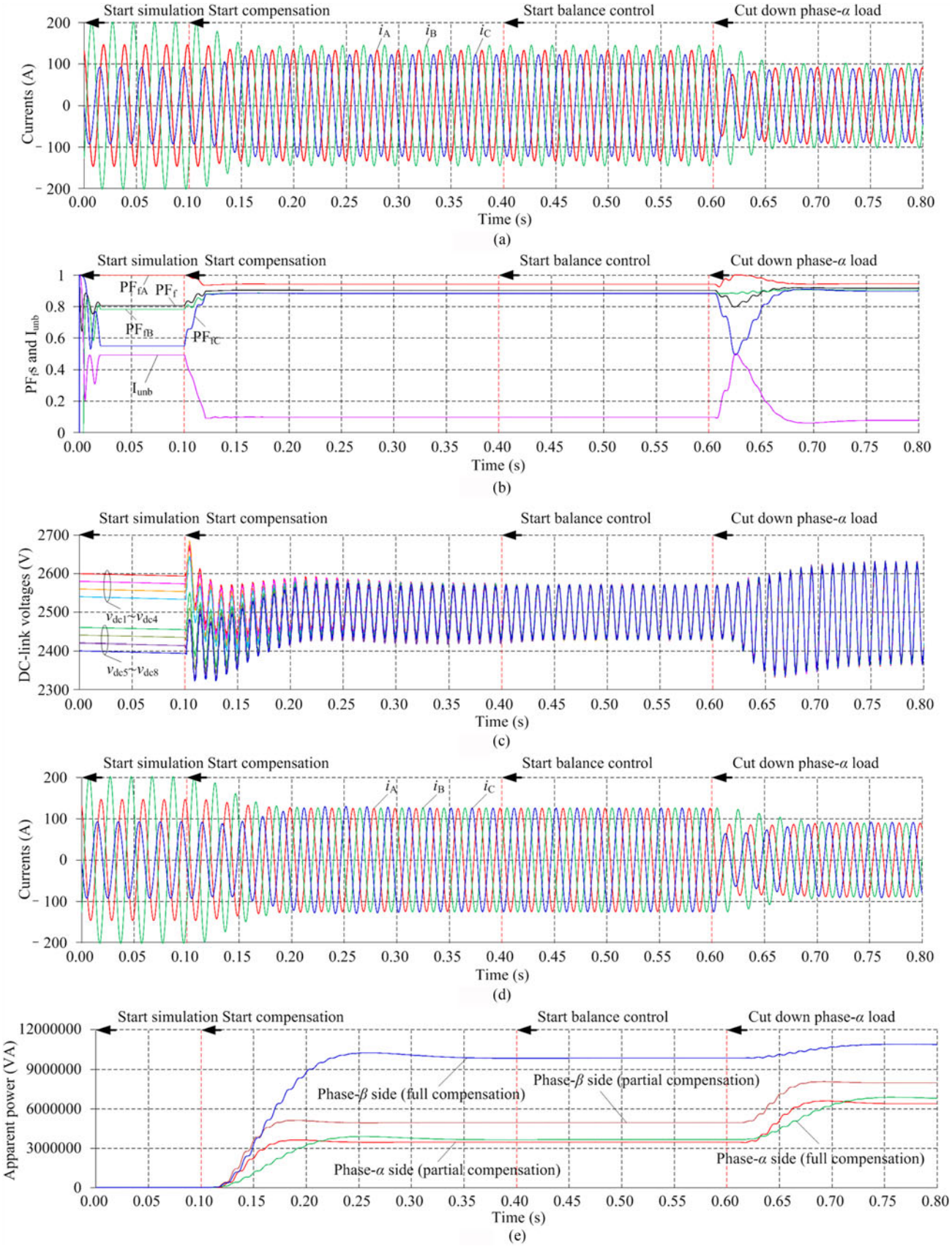

Fig. 8. Simulation results. (a) Primary current waveforms under partial compensation. (b) $\mathrm{PF_{fs}}$ ($\mathrm{PF_f}$, $\mathrm{PF_{fA}}$, $\mathrm{PF_{fB}}$, and $\mathrm{PF_{fC}}$) and I_{unb} under partial compensation. (c) DC-link voltage waveforms under partial compensation. (d) Primary current waveforms under full compensation. (e) Compensation apparent power of each side under different compensation modes.

TABLE II
SIMULATION RESULTS STATISTICS OF THE STEADY STATES

Items		Partial	Full
Before compensation	I_{unb} (%)	49	49
	$\mathrm{PF_f}$	0.8	0.8
	S_α (MVA)	0	0
	S_β (MVA)	0	0
After compensation	I_{unb} (%)	9.5	0.35
	$\mathrm{PF_f}$	0.902	0.99
	S_α (MVA)	3.4	3.78
	S_β (MVA)	6.5	10.16
After loads change	I_{unb} (%)	8.5	1.03
	$\mathrm{PF_f}$	0.915	0.99
	S_α (MVA)	5.0	6.85
	S_β (MVA)	8.2	11.22

comprehensive index for reactive power on the primary side, not for the individual phases, so the power factor of each phase on the primary side ($\mathrm{PF_{fA}}$, $\mathrm{PF_{fB}}$, and $\mathrm{PF_{fC}}$ in Fig. 8(b)) is different from $\mathrm{PF_f}$. The units' dc-link voltages are set near to the reference value and slightly different at the beginning, as shown in Fig. 8(c). The dc-link overall voltage is held due to the overall voltage control, and the balance condition of the units' dc-link voltages is improved because of the self-balance capability, but the differences of the units' dc-link voltages are not eliminated until the balance control is activated at 0.4 s. When the load on phase α is cut down at 0.6 s, a transient process from one steady state to another occurs, and almost no oscillation appears on the primary currents and dc-link voltages. The dynamical performance is satisfactory.

As a comparison, the primary three-phase currents under full compensation condition (see Fig. 8(d)) are also presented. However, the required power ratings are much higher than that of partial compensation mode (see Fig. 8(e)). Specifications are listed in Table II (note, all the data are recorded on the condition that the grid three-phase voltage sources are set 10% higher than the nominal voltage listed in Table I).

B. Experimental Verification

To further verify the correctness of the proposed system, two experimental setups rated at 2 kVA have been built up in the laboratory. Fig. 9 is the experimental wiring diagrams and Table III gives the specifications of experimental systems' parameters. One point should be noticed here is that the coupling transformer, which is expected to act as an isolation and voltage-matching stage for phase-α side converter, is replaced 1) by an autotransformer on single BTBC occasion (see Fig. 9(a)), and 2) by a combination of a autotransformer and a normal single-phase three-winding transformer on dual BTBCs ($\mathrm{BTBC_1}$ and $\mathrm{BTBC_2}$) occasion (see Fig. 9(b)).

Fig. 10 demonstrates the experimental results of the single BTBC occasion in Fig. 9(a). From Fig. 10(a), (b), (e), and (f), we can know that the transient processes during the start on and loads change stages are satisfactory and the steady states on different load conditions are excellent. For the dc-link voltage, no overshoot and oscillation appear at transient situation, especially

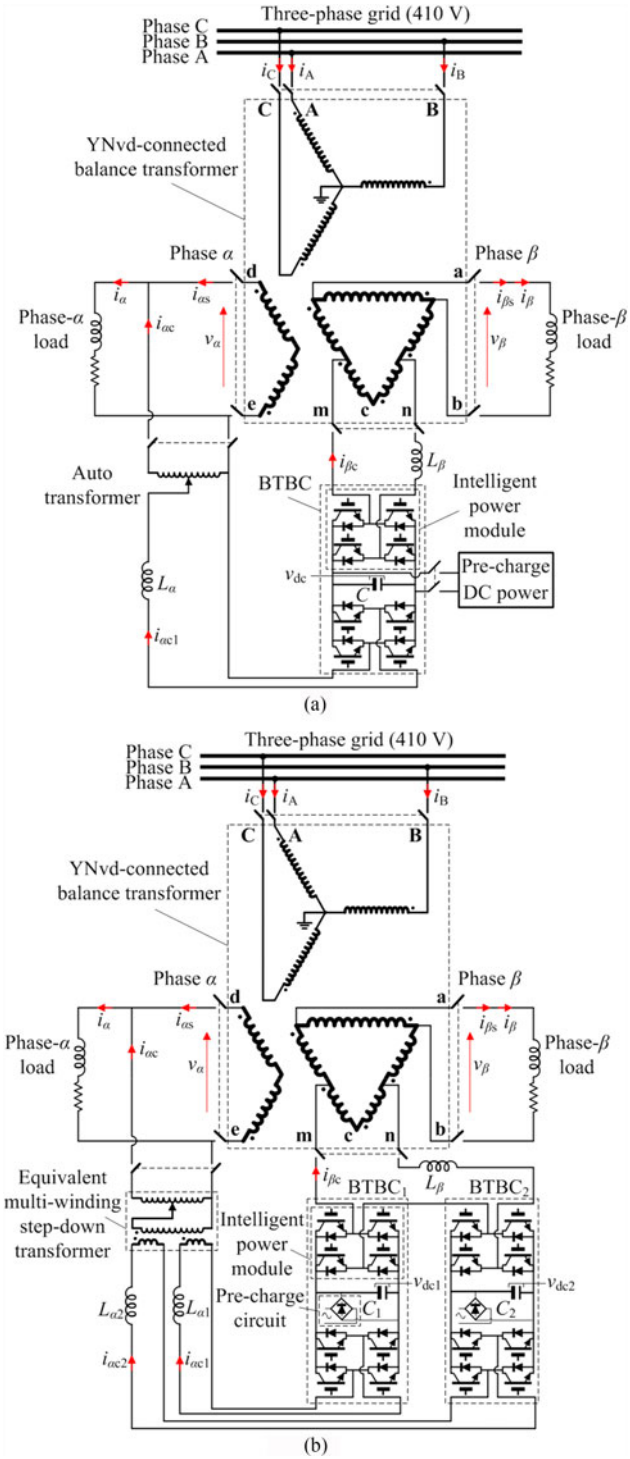

Fig. 9. Experimental wiring diagrams. (a) Single BTBC occasion. (b) Dual BTBCs occasion.

when loads change (see Fig. 10(c), (d), (g), and (h)). The energy needed for raising the dc-link voltage from the precharge to the reference value, when the compensation is enabled, is considered to be responsible for the slight overshoot of the primary currents (see Fig. 10(a) and (e)). Besides, the rippled dc-link voltage of full-compensation mode is slightly larger than that

TABLE III
EXPERIMENTAL SYSTEMS' PARAMETERS

Items	Parameters	Value
YNvd-connected balance transformer	Primary line voltage	410 V
	Capacity	2 kVA
	K (transformer ratio)	577/220
Current sensor	Transformation ratio	100 A/50 mA
Load in phase α	Resistor	25 Ω / 9.2 kW
Load in phase β	Resistor-reactor	$(7 + 6.28\mathrm{j})\Omega/20\mathrm{A}$
Inductance	L_α	3 mH/20 A
	$L_{\alpha 1}$, $L_{\alpha 2}$	1 mH/20 A
	L_β	5 mH/20 A
Capacitance	C	4.5 mF/700 V
	C_1, C_2	3 mF/700 V
Intelligent power module (PM50RLA120)	Nominal rating	50 A/1200 V
Controller	Digital chip	TMS320F28335
	Sample frequency	10 kHz
	B	50 Ω
DC-link	Reference	110 V (overall)
		55 V (individual)
	Precharge	83 V (for C)
		53 V (for C_1)
		43 V (for C_2)
PI regulator for dc-link overall voltage control	Proportional gain	2
	Integral gain	5
PI regulator for dc-link voltage balance control	Proportional gain	0.2
	Integral gain	1

TABLE IV
EXPERIMENTAL RESULTS STATISTICS OF THE STEADY STATES ON SINGLE BTBC OCCASION

Items		Partial	Full
Before compensation	I_{unb} (%)	46.51	46.51
	$\mathrm{PF_f}$	0.8026	0.8026
	S_α (VA)	0	0
	S_β (VA)	0	0
After compensation	I_{unb} (%)	10.01	0.58
	$\mathrm{PF_f}$	0.9017	0.9995
	S_α (VA)	224	210
	S_β (VA)	398	844
After loads change	I_{unb} (%)	9.23	0.37
	$\mathrm{PF_f}$	0.9058	–0.9982
	S_α (VA)	358	463
	S_β (VA)	590	889

of the partial-compensation mode. This is because the power delivered on full-compensation condition is larger than the one on partial-compensation situation, which is demonstrated by Fig. 10(i) (note: in order to facilitate the presentation and comparison of the apparent power, the experimental data recorded by the power quality analyzer HIOKI 3198 (one data per second) are plotted in Excel). Table IV lists the specifications of the experimental results. It can be seen from Table IV that before compensation, $I_{\mathrm{unb}} = 46.51\%$ and $\mathrm{PF_f} = 0.8026$; when the partial compensation is activated, $\mathrm{PF_f}$ improves to 0.917 and

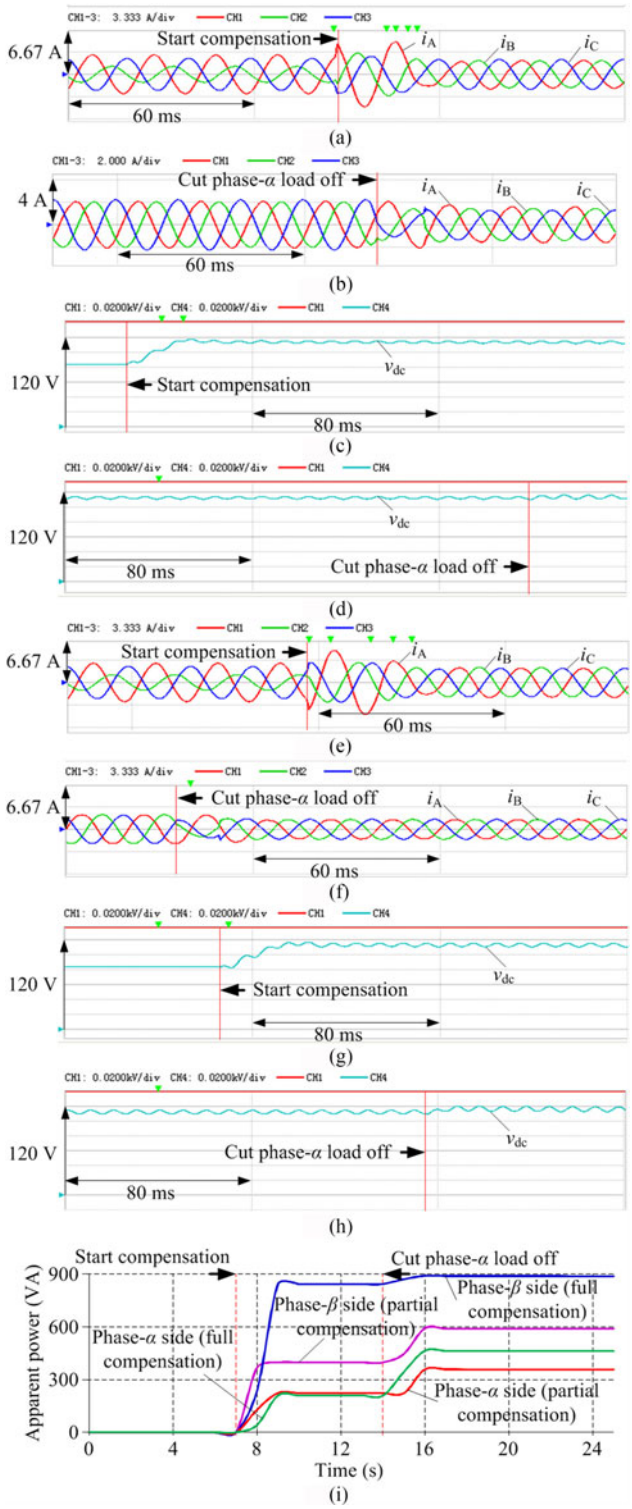

Fig. 10. Experimental results on single BTBC occasion. (a) Primary current waveforms at the beginning of partial compensation. (b) Primary current waveforms under partial compensation when loads change. (c) DC-link voltage waveform at the beginning of partial compensation. (d) DC-link voltage waveform under partial compensation when loads change. (e) Primary current waveforms at the beginning of full compensation. (f) Primary current waveforms under full compensation when loads change. (g) DC-link voltage waveform at the beginning of full compensation. (h) DC-link voltage waveform under full compensation when loads change. (i) Compensation apparent power of each side under different compensation modes.

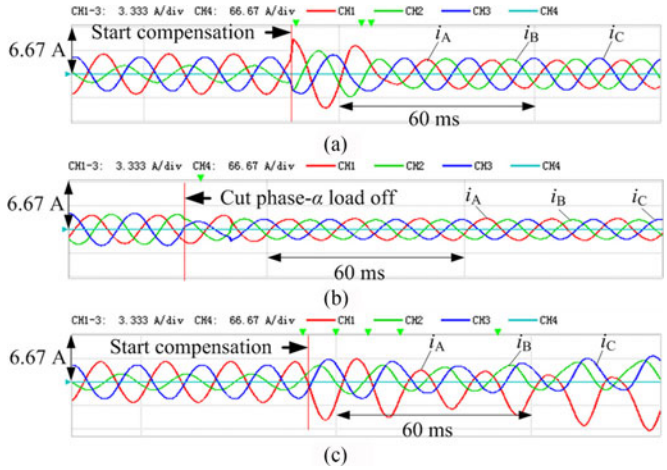

Fig. 11. Experimental results on single BTBC occasion for stability verification. (a) Primary current waveforms at the beginning of partial compensation ($L_\beta = 3$ mH). (b) Primary current waveforms under partial compensation when loads change ($L_\beta = 3$ mH). (c) Primary current waveforms at the beginning of partial compensation (a delay in the acquisition of $\mathbf{x}$ is introduced).

TABLE V
EXPERIMENTAL RESULTS STATISTICS OF THE STEADY STATES ON DUAL BTBCS OCCASION

Items		Partial	Full
Before compensation	I_{unb} (%)	46.54	46.54
	$\mathrm{PF_f}$	0.8033	0.8033
	S_α (VA)	0	0
	S_β (VA)	0	0
After compensation	I_{unb} (%)	10.11	0.48
	$\mathrm{PF_f}$	0.9022	0.9996
	S_α (VA)	225	213
	S_β (VA)	402	846
After loads change	I_{unb} (%)	9.22	0.40
	$\mathrm{PF_f}$	0.9055	–0.9983
	S_α (VA)	360	465
	S_β (VA)	593	892

the index I_{unb} decreases from 46.51% to 10.01%, which means the expected compensation performance is achieved.

For the stability aspects discussed in Section III, it can be seen from Fig. 11(a) and (b) that no deteriorated performance appears when L_β changes from 5 to 3 mH. While the system shows unstable performance (see Fig. 11(c)) if a delay is introduced in the acquisition of $\mathbf{x}$.

For the dual BTBCs occasion in Fig. 9(b), the experimental results are presented in Fig. 12 and Table V. From Fig. 12 and Table V, it can be seen that the experimental results on this topology show no significant difference to that on the former topology. Besides, the system exhibits its unit dc-link voltage self-balance capability in Fig. 12(e), though the balance performance is not as good as that when the balance control scheme is adopted (see Fig. 12(f)). Note: because the unit dc-link voltage reference on this topology is 0.5 times to the former topology's dc-link voltage reference, the ripples of the unit dc-link voltage are slightly larger than that shown in Fig. 10.

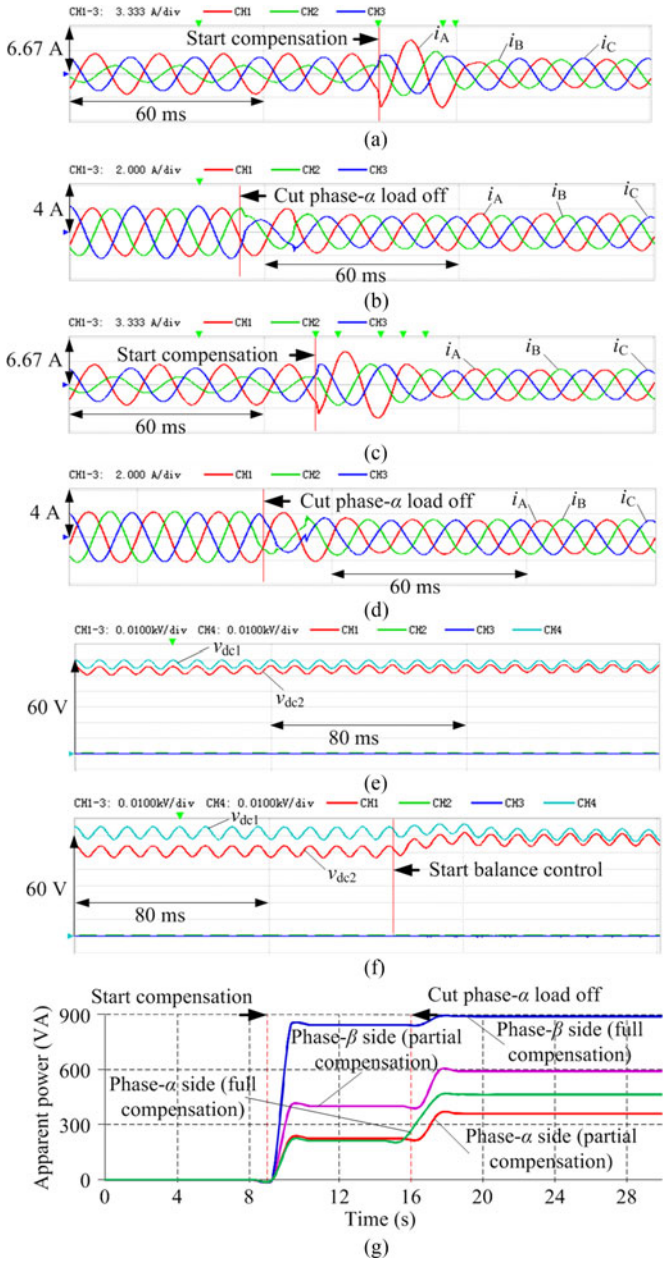

Fig. 12. Experimental results on dual BTBCs occasion. (a) Primary current waveforms at the beginning of partial compensation. (b) Primary current waveforms under partial compensation when loads change. (c) Primary current waveforms at the beginning of full compensation. (d) Primary current waveforms under full compensation when loads change. (e) DC-link voltage waveforms without balance control. (f) DC-link voltage waveforms with balance control. (g) Compensation apparent power of each side under different compensation modes.

V. CONCLUSION

Based on the theoretical discussion presented in the first part of this paper, this paper mainly focuses on the implementation and verification of the proposed system. The system modeling is briefly introduced; the passivity-based control scheme is also discussed in detail, including the design of the current controller, stability analysis, the overall and unit dc-link voltage control. In addition, a simulation model is established and two sets of

experimental systems are physically implemented. All the results verify the theoretical analysis. Considering the features like high level of modularity, and integration, relatively low compensating capacity, the MBTBC-YNvd transformer-integrated system is cost efficiency for power quality improvement in ERPS.

APPENDIX A

The partial compensation goals (defined in the first part of this paper) are

$$\begin{cases} PF_f = \sum_{k=A,B,C} P_k \Big/ \sum_{k=A,B,C} S_k \\ \qquad = \sum_{k=A,B,C} I_{kp} \Big/ \sum_{k=A,B,C} I_k \geq 0.9 \\ I_{\mathrm{unb}} = I_- / I_+ \times 100\% \leq 10\% \end{cases} \tag{A1}$$

where $\mathrm{PF_f}$ and I_{unb} mean the fundamental power factor and NSC unbalance ratio, separately; P_k and S_k are the fundamental active power and apparent power of the primary three phases, respectively; I_k is the amplitude of the fundamental primary three-phase currents; I_{kp} represents the amplitude of the active power components of I_{k}; and I_- and I_+ denote the amplitude of the fundamental NSC and positive-sequence current, separately.

REFERENCES

[1] F. Ciccarelli, M. Fantauzzi, D. Lauria, and R. Rizzo, "Special transformers arrangement for AC railway systems," in *Proc. Electr. Syst. Aircr., Railw, Ship Propulsion Conf.*, 2012, pp. 16–18.

[2] F. Ma, A. Luo, X. Xu, H. Xiao, C. Wu, and W. Wang, "A simplified power conditioner based on half-bridge converter for high-speed railway system," *IEEE Trans. Ind. Electron.*, vol. 60, no. 2, pp. 728–738, Feb. 2013.

[3] S. R. Sama, S. Paul, and S. H. N. Dey, "Elimination of partial overloading of generators under unbalanced operating conditions of power systems," *CSEE J. Power Energy Syst.*, vol. 2, no. 1, pp. 81–87, Mar. 2016.

[4] R. E. Morrison, "Power quality issues on ac traction systems," in *Proc. Rec. 9th Int. Conf. Harmon. Qual. Power*, 2000, pp. 709–714.

[5] L. He, J. Xiong, H. Ouyang, P. Zhang, and K. Zhang, "High-performance indirect current control scheme for railway traction four-quadrant converters," *IEEE Trans. Ind. Electron.*, vol. 61, no. 12, pp. 6645–6654, Dec. 2014.

[6] H. Hu, Z. He, and S. Gao, "Passive filter design for China high-speed railway with considering harmonic resonance and characteristic harmonics," *IEEE Trans. Power Del.*, vol. 30, no. 1, pp. 505–514, Feb. 2015.

[7] Z. He, H. Hu, Y. Zhang, and S. Gao, "Harmonic resonance assessment to traction power-supply system considering train model in China high-speed railway," *IEEE Trans. Power Del.*, vol. 29, no. 4, pp. 1735–1743, Aug. 2014.

[8] S. M. M. Gazafrudi, A. T. Langerudy, E. F. Fuchs, and K. AI-Haddad, "Power quality issues in railway electrification: A comprehensive perspective," *IEEE Trans. Ind. Electron.*, vol. 62, no. 5, pp. 3081–3090, May 2015.

[9] L. Morán, C. Albistur, and R. Burgos, "Multi-mega VAR passive filters for mining applications: Practical limitations and technical considerations," in *Proc. IEEE Ind. Appl. Soc. Annu. Meet.*, 2015, pp. 1–8.

[10] S. Bhattacharya, P. T. Cheng, and D. M. Divan, "Hybrid solutions for improving passive filter performance in high power applications," *IEEE Trans. Ind. Appl.*, vol. 33, no. 3, pp. 732–747, May/Jun. 1997.

[11] H. Akagi, "Active harmonic filters," *Proc. IEEE*, vol. 93, no. 12, pp. 2128–2141, Dec. 2005.

[12] Y. Li *et al.*, "A virtual impedance comprehensive control strategy for the controllably inductive power filtering system," *IEEE Trans. Power Electron.*, vol. 32, no. 2, pp. 920–926, Feb. 2017.

[13] Y. Li, T. K. Saha, O. Krause, Y. Cao, and C. Rehtanz, "An inductively active filtering method for power-quality improvement of distribution networks with nonlinear loads," *IEEE Trans. Power Del.*, vol. 28, no. 4, pp. 2465–2473, Oct. 2013.

[14] S. Buso, L. Malesani, and P. Mattavelli, "Comparison of current control techniques for active filter applications," *IEEE Trans. Ind. Electron.*, vol. 45, no. 5, pp. 722–729, Oct. 1998.

[15] B. Singh, R. Saha, A. Chandra, and K. Al-Haddad, "Static synchronous compensators (STATCOM): A review," *IET Power Electron.*, vol. 2, no. 4, pp. 297–324, 2009.

[16] Z. Chen, J. M. Guerrero, and F. Blaabjerg, "A review of the state of the art of power electronics for wind turbines," *IEEE Trans. Power Electron.*, vol. 24, no. 8, pp. 1859–1875, Aug. 2009.

[17] S. Yang, Y. Liu, X. Wang, D. Gunasekaran, U. Karki, and F. Z. Peng, "Modulation and control of transformer-less UPFC," *IEEE Trans. Power Electron.*, vol. 31, no. 2, pp. 1050–1063, Feb. 2016.

[18] S. B. Karanki, N. Geddada, M. K. Mishra, and B. K. Kumar, "A modified three-phase four-wire UPQC topology with reduced DC-link voltage rating," *IEEE Trans. Ind. Electron.*, vol. 60, no. 9, pp. 3555–3566, Sep. 2013.

[19] R. Bhavani, N. R. Prabha, and C. Kanmani, "Fuzzy controlled UPQC for power quality enhancement in a DFIG based grid connected wind power system," in *Proc. Int. Conf. Circuit, Power Comput. Technol.*, 2015, pp. 1–7.

[20] M. P. Kazmierkowski and L. Malesani, "Current control techniques for three-phase voltage-source PWM converters: A survey," *IEEE Trans. Ind. Electron.*, vol. 45, no. 5, pp. 69–703, Oct. 1998.

[21] M. Monfared, S. Golestan, and J. M. Guerrero, "Analysis, design, and experimental verification of a synchronous reference frame voltage control for single-phase inverters," *IEEE Trans. Ind. Electron.*, vol. 61, no. 1, pp. 258–269, Jan. 2014.

[22] Z. Sun, X. Jiang, D. Zhu, and G. Zhang, "A novel active power quality compensator topology for electrified railway," *IEEE Trans. Power Electron.*, vol. 19, no. 4, pp. 1036–1042, Jul. 2004.

[23] A. Bueno, J. M. Aller, J. A. Restrepo, R. Harley, and T. G. Habetler, "Harmonic and unbalance compensation based on direct power control for electric railway systems," *IEEE Trans. Power Electron.*, vol. 28, no. 12, pp. 5823–5831, Dec. 2013.

[24] S. Hu, Z. Zhang, Y. Li, L. Luo, Y. Cao, and C. Rehtanz, "A new half-bridge winding compensation-based power conditioning system for electric railway with LQRI," *IEEE Trans. Power Electron.*, vol. 29, no. 10, pp. 5242–5256, Oct. 2014.

[25] S. Hu *et al.*, "A new integrated hybrid power quality control system for electrical railway," *IEEE Trans. Ind. Electron.*, vol. 62, no. 10, pp. 6222–6232, Oct. 2015.

[26] S. Tamai, "Novel power electronics application in traction power supply system in Japan," in *Proc. Int. Power Electron. Motion Control Conf. Expo.*, 2014, pp. 701–706.

[27] K. Kunomura *et al.*, "Electronic frequency converter feeding single-phase circuit and controlling feeder voltage with fixed power factor method for Shinkansen," *IEEE Trans. Power Electron.*, vol. 27, no. 9, pp. 3888–3896, Sep. 2012.

[28] D. Zhang, Z. Zhang, W. Wang, and Y. Yang, "Negative sequence current optimizing control based on railway static power conditioner in V/v traction power supply system," *IEEE Trans. Power Electron.*, vol. 31, no. 1, pp. 200–212, Jan. 2016.

[29] R. Ortega, A. Loría, P. J. Nicklasson, and H. Sira-Ramírez, *Passivity-Based Control of Euler-Lagrange Systems: Mechanical, Electrical and Electromechanical Applications*. London, U.K.: Springer-Verlag, 1998.

[30] R. Xu *et al.*, "A novel control method for transformerless H-bridge cascaded STATCOM with star configuration," *IEEE Trans. Power Electron.*, vol. 30, no. 3, pp. 1189–1202, Mar. 2015.

[31] R. Rahmani, A. Hamadi, and K. AI-Haddad, "A Lyapunov-function-based control for a three-phase shunt hybrid active filter," *IEEE Trans. Ind. Electron.*, vol. 59, no. 3, pp. 1418–1429, Mar. 2012.

[32] S. Hu *et al.*, "A Y-D multifunction balance transformer-based power quality control system for single-phase power supply system," *IEEE Trans. Ind. Appl.*, vol. 52, no. 2, pp. 1270–1279, Mar./Apr. 2016.

[33] B. Xie, Z. Zhang, S. Hu, Y. Li, L. Luo, and S. Sun, "YN/VD connected balance transformer-based electrical railway negative sequence current compensation system with passive control scheme," *IET Power Electron.*, vol. 9, no. 10, pp. 2044–2051, 2016.

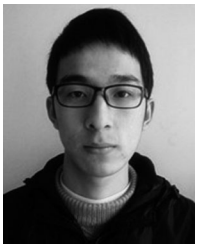

Bin Xie was born in Hunan, China, in 1990. He received the B.Sc. degree in electrical engineering from Shaoyang University, Shaoyang, China, in 2013. He is currently working toward the Ph.D. degree in electrical engineering at the College of Electrical and Information Engineering, Hunan University, Changsha, China.

His research interests include power quality analysis and compensation strategy of electrical railway power systems, renewable energy, and high-power applications of converters.

Zhiwen Zhang received the B.Sc. and M.Sc. degrees in electrical engineering and the Ph.D. degree in control theory and control engineering from Hunan University, Changsha, China, in 1987, 1990, and 2006, respectively.

From 1992 to 1993 and 2006 to 2007, he was a Visiting Scholar with Tsinghua University, Beijing, China, and a Visiting Professor with Ryerson University, Toronto, Canada, respectively. He is currently a Full Professor with the College of Electrical and Information Engineering, Hunan University. His research interests include theory and new technology of ac/dc energy transform, theory and application of new-type electric apparatus, harmonic suppression for electric railway, power electronics application, and computer control.

Yong Li (S'09–M'12–SM'14) was born in Henan, China, in 1982. He received the B.Sc. and Ph.D. degrees from the College of Electrical and Information Engineering, Hunan University, Changsha, China, in 2004 and 2011, respectively. He received the second Ph.D. degree from the Institute of Energy Systems, Energy Efficiency, and Energy Economics (ie3), TU Dortmund University, Dortmund, Germany, in June 2012.

In 2009, he was a Research Associate with ie3. After then, he was a Research Fellow with The University of Queensland, Brisbane, Australia. Since 2014, he has been a Full Professor of electrical engineering with Hunan University. His current research interests include power system stability analysis and control, ac/dc energy conversion systems and equipment, analysis and control of power quality, and HVdc and FACTS technologies.

Dr. Li is a Member of the Association for Electrical, Electronic and Information Technologies in Germany.

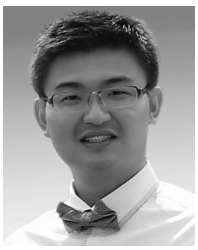

Sijia Hu (S'14–M'16) was born in Hunan, China, in 1987. He received the B.Sc. degree in electrical engineering (and automation) from Hunan University of Science and Technology, Xiangtan, China, in 2010, and the Ph.D. degree in electrical engineering (and automation) from Hunan University (HNU), Changsha, China, in 2015.

Since 2016, he has been an Assistant Professor of electrical engineering with HNU. His research interests include power flow and power quality control of electric railway power systems, new topology converters, and stability and power quality analyses and control of multiconverter systems.

Longfu Luo (M'09) was born in Hunan, China, in 1962. He received the B.Sc., M.Sc., and Ph.D. degrees from the College of Electrical and Information Engineering, Hunan University, Changsha, China, in 1983, 1991, and 2001, respectively.

From 2001 to 2002, he was a Senior Visiting Scholar with the University of Regina, Regina, SK, Canada. He is currently a Full Professor of electrical engineering with the College of Electrical and Information Engineering, Hunan University. His research interests include the design and optimization of modern electrical equipment, the development of new converter transformer, and the study of corresponding new HVDC theories.

Christian Rehtanz (M'96–SM'06) was born in Germany in 1968. He received the Diploma and Ph.D. degrees in electrical engineering from TU Dortmund University, Dortmund, Germany, in 1994 and 1997, respectively. He received the *venia legend* in electrical power systems from the Swiss Federal Institute of Technology, Zurich, Switzerland, in 2003.

In 2000, he joined ABB Corporate Research, Baden, Switzerland. He became the Head of Technology for the global ABB business area of power systems in 2003, and the Director of ABB Corporate Research, Beijing, China, in 2005. Since 2007, he has been the Head of the Institute of Energy Systems, Energy Efficiency and Energy Economics, TU Dortmund University. In addition, he has been a Scientific Advisor of ef.Ruhr GmbH, Dortmund, a joint research company of the three universities of Bochum, Dortmund, and Duisburg-Essen (University Alliance Metropolis Ruhr) since 2007. He is an Adjunct Professor with Hunan University, Changsha, China. He has authored more than 150 scientific publications, three books, and 17 patents and patent applications. His research interests include electrical power systems and power economics, technologies for network enhancement and congestion relief, such as stability assessment, wide-area monitoring, protection, and coordinated network control, and integration and control of distributed generation and storage.

Dr. Rehtanz received the MIT World Top 100 Young Innovators Award in 2003.

Olav Krause (M'05) was born in Germany in 1978. He received the Dipl.Ing. (M.E.) and Dr. Ing. (Ph.D.) degrees in electrical engineering from TU Dortmund University, Dortmund, Germany, in 2005 and 2009, respectively.

He is currently a Lecturer of electrical engineering with the School of Information Technology and Electrical Engineering, The University of Queensland, Brisbane, Qld., Australia. His main research interests include distribution network automation, with a focus on state estimation under measurement deficiency and power system load ability determination. This is complemented by work on techniques of probabilistic and harmonic power-flow analysis.